Digital microscopic mapping of laser induced polarization ellipticity maps in differential diagnostics of preparations of benign and malignant prostate tumours

Trifonyuk[1] L., Strashkevich[2] A., Kozlov[1] S., Davidenko[1] I., Poliansky[1] I., Pavlyukovich[1] N., Pavlyukovich[1] A., Tomka[3] Yu., Fesiv[3] I.V., Yu.A. Ushenko[3],M. Talakh[3], P.A. Gorodenskiy[3], V.K. Gantyuk[3]
[1] Bukovinian State Medical University, Chernivtsi, Ukraine
[2]The Institute of Traumatology and Orthopedics by NAMS of Ukraine, Kyiv, Ukraine
[3]Chernivtsi National University, Chernivtsi, Ukraine

ABSTRACT

The article presents the results of a study of the possibilities of 3D Stokes-polarimetric mapping [1-5] of microscopic images of protein fluorofors of the prostate. Polarization-holographic measurement and analysis of layer-by-layer maps and histograms of the distribution of the polarization ellipticity of microscopic images of biological preparations of the prostate. Determination of the relationship between statistical moments of the 1st - 4th orders [6,7], which characterize layer-by-layer maps of distributions of the polarization ellipticity of microscopic images of biological preparations of the prostate and pathological conditions of the prostate. Determination of the operational characteristics (sensitivity, specificity, accuracy) of the diagnostic strength of the 3D layer-by-layer Stokes polarimetric mapping method [8,9].

Keywords: polarization, diagnostics, tumor, statistical moments, interferometry.

1. STRUCTURAL-LOGICAL AND OPTICAL SCHEME OF 3D LAYER-BY-LAYER STOKES-POLARIMETRY OF MICROSCOPIC IMAGES OF BIOLOGICAL PREPARATIONS

In fig. 1 shows the structural-logical diagram and design of the method of 3D layer-by-layer Stokes-polarimetry [10-13]of microscopic images of histological sections of biopsy of prostate tumorus.

1	Optical probing source	Gas helium-neon laser; Wavelength 0.6328 μm Power 10 mW
2	Block for forming the spatial structure of the optical probe	Optical collimator for forming a parallel laser beam with a cross section of 5 mm
3	Multichannel block for the formation of the polarization structure of the optical probe	System of formation of linear (0^0;90^0;45^0) and right-circular polarization.
4	Object block	Microscopic coordinate node
5	Formation block of microscopic image	Polarizing micro lens
6	Multichannel polarization filtering block	Transmission system of linearly (0^0;90^0;45^0;135^0), right- and left-circularly polarized components
7	Reference coherent wave formation block	Polarizing beam splitter
8	Multichannel block for the formation of the polarization structure of the reference coherent wave	System of left and right polarization (0^0;90^0;45^0)
9	Polarization filtering block for interference distributions	Linear polarizer
10	Discritization block of polarization-	Digital CCD camera

Fifteenth International Conference on Correlation Optics, edited by Oleg V. Angelsky, Proc. of SPIE Vol. 12126, 1212627
© 2021 SPIE · 0277-786X · doi: 10.1117/12.2616835

	interference distribution in the plane of a digital microscopic image	(The Imaging Source DMK 41AU02.AS, monochrome 1/2 "CCD, Sony ICX205AL (progressive scan); resolution - 1280x960, size light-sensitive area - 7600x6200mkm; sensitivity - 0.05 lx, dynamic range - 8 bit, SNR - 9 bit) by polarization microobjective 7 (Nikon CFI Achromat P, focal length - 30 mm, numerical aperture - 0.1 increase - 4x)
11	Block for computer processing of polarization interferometry data	Calculation algorithms: - distributions of the magnitude of the ellipticityof polarization of the microscopic image; - statistical moments of the 1st - 4th orders characterizing the polarization maps.

Fig. 1. Structural-logical diagram of the method of 3D layer-by-layer Stokes-polarimetry of microscopic images of histological sections of biopsy of prostate tumours.

The optical location of the method of polarization interferometry of microscopic images of histological sections of biopsy of prostate tumors is illustrated in Fig. 2 [14-19].

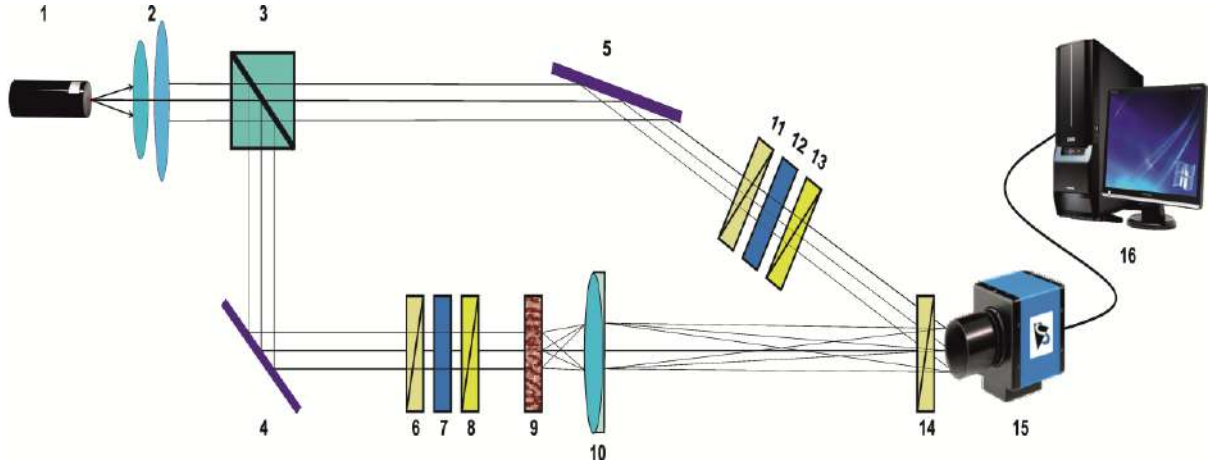

Fig. 2. Optical scheme of 3D Stokes-polarimetry of microscopic images of histological sections of biopsy of prostate tumours.

Collimator 2 forms a parallel ($\varnothing = 2 \times 10^3 \mu m$) beam of He-Ne ($\lambda = 0{,}6328 \mu m$) laser 1, which is divided by 50% beam splitter 3 into "irradiating" (*Ir*) and "reference" (Re).

The "irradiating" by the rotating mirror 4 is directed through the polarizing filter 6 - 8 in the direction of the sample of the biological layer 9 [20-25].

The polarization-inhomogeneous image of the object 9 by the lens 10 is projected into the plane of the digital camera 15.

The "reference" beam is directed by the mirror 5 through the polarizing filter 11 - 13 into the image plane of the object 9.

The resulting interference pattern is recorded by a digital camera 15 through a polarizer 14.

2. TECHNIQUE OF 3D LAYER-BY-LAYER POLARIZATION-HOLOGRAPHIC MAPPING OF POLARIZATION MAPS

Experimental studies include the following set of actions:

1. Formation of coplanar polarization states in the "irradiating" and "reference" laser beams (Fig. 2).

2. Registration of two partial interference patterns through a polarizer-analyzer 14 with an orientation of the transmission plane at angles $\Omega = 0^0;\quad \Omega = 90^0$ (Fig. 2).

3. For each partial interference distribution, we perform a two-dimensional discrete Fourier transform on the image.

4. Applying a two-dimensional inverse discrete Fourier transform on the obtained spectrum of complex amplitudes and phases of a microscopic image of a biological layer.

5. We apply the analytical operation of phase scanning and obtain a set of layer-by-layer distributions of complex amplitudes and phases of a microscopic image of a biological layer.

6. We use the well-known algorithm for determining the distributions of the Stokes vector $S_{i=1;2;3;4}(\theta_k, x, y)$ parameters with algorithmic reproduction of the polarization ellipticity maps $\alpha(\theta_k, x, y)$ in each phase plane θ_k [17,18].

$$\alpha(\theta_k, x, y) = 0{,}5\text{arctg}\left[\frac{S_4(\theta_k, x, y)}{S_1(\theta_k, x, y)}\right]. \tag{1}$$

3. COORDINATE AND STATISTICAL STRUCTURE OF LAYERED ELLIPTICITY MAPS OF POLARIZATION OF MICROSCOPIC IMAGES OF BIOLOGICAL PREPARATIONS OF PROSTATE TUMORS OF VARIOUS DIFFERENTIATION

Coordinate (fragments (1)) and statistical parameters of histograms (fragments (2)) of the distributions of the polarization ellipticity of digital microscopic images of histological sections of biopsy of adenoma and adenocarcinoma with different degrees of differentiation are shown in a series of fragments in Fig. 3 - Fig. 6.

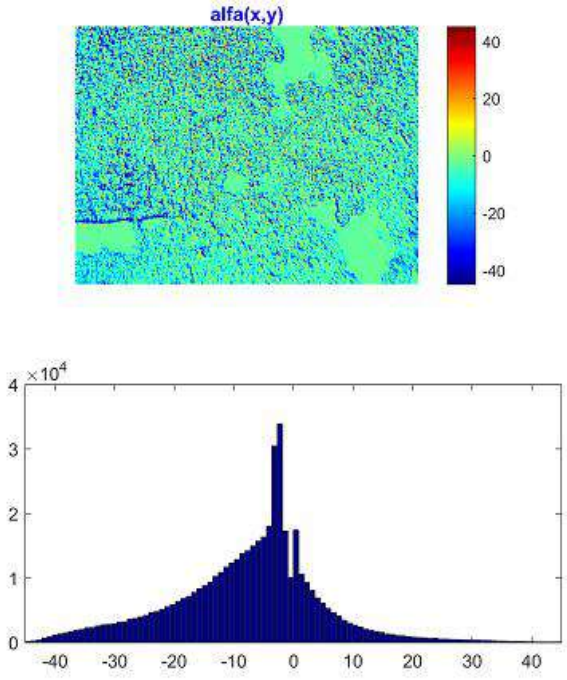

Fig. 3. Topographic map (fragment (1)) and histogram of layer-by-layer distribution (fragment (2)) of the polarization ellipticity of a digital microscopic image of a histological section of adenoma biopsy - control group 1.

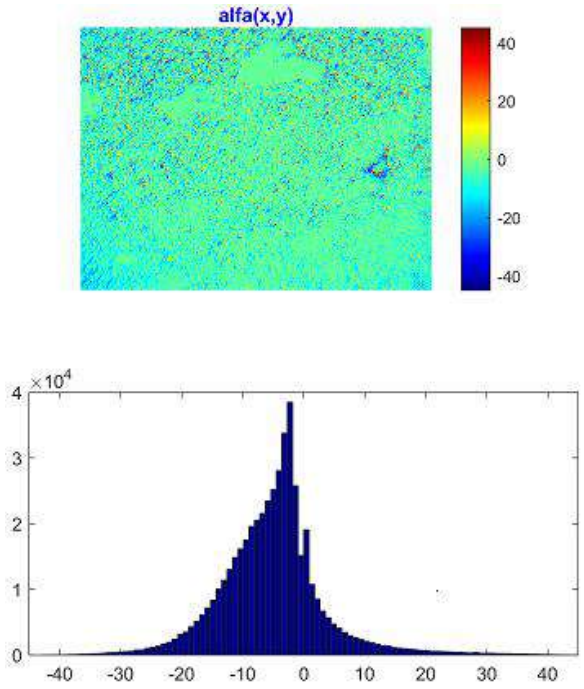

Fig. 4. Topographic map (fragment (1)) and histogram of layer-by-layer distribution (fragment (2)) of the polarization ellipticity of a digital microscopic image of a histological section of a biopsy of a highly differentiated adenocarcinoma (3 + 3) - research group 2.

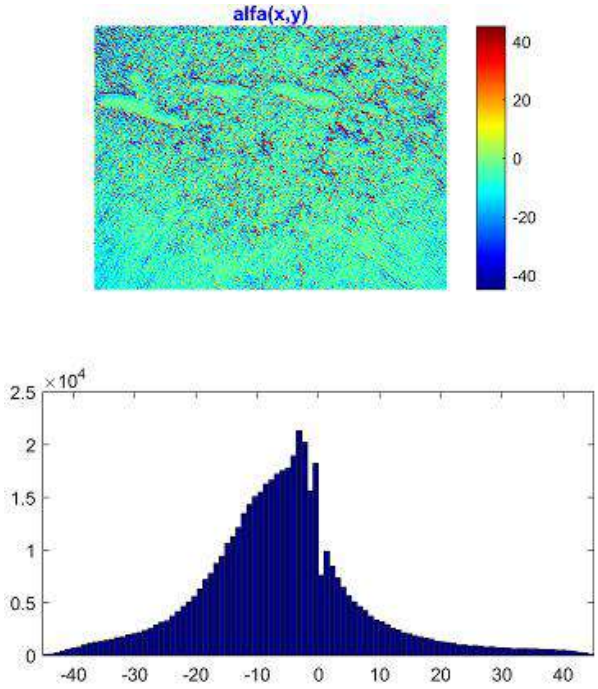

Fig. 5. Topographic map (fragment (1)) and histogram of layer-by-layer distribution (fragment (2)) of the polarization ellipticity of a digital microscopic image of a histological section of a biopsy of a mid-differentiation adenocarcinoma (3 + 4) - research group 3.

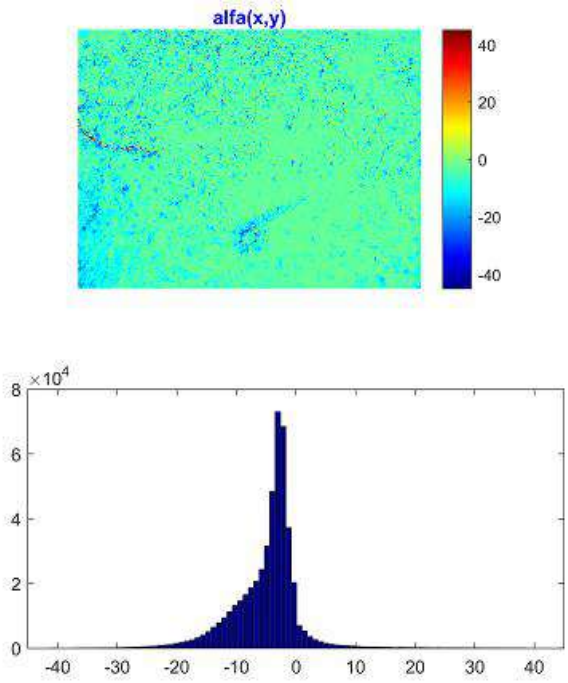

Fig. 6. Topographic map (fragment (1)) and histogram of layer-by-layer distribution (fragment (2)) of the polarization ellipticity of a digital microscopic image of a histological section of a biopsy of a low differentiation adenocarcinoma (4 + 4) - control group 4.

Comparative analysis of the results of 3D layer-by-layer polarization-holographic measurement of polarization ellipticity maps (Fig. 3 - Fig. 6) of microscopic images of biological preparations of representative samples of all types of prostate tissue tumors revealed an individual structure and a consistent decrease in the average histograms of layer-by-layer distributions of polarization ellipticity in the plane of digital microscopic images samples of histological sections biopsy of adenoma and adenocarcinoma as the degree of differentiation on the Gleason scale decreases – (3+3), (3+4) i (4+4).

Biophysical, this can be associated with necrotic changes in the morphological structure of malignant prostate tumours, which lead to a decrease in the level of optical anisotropy of histological sections of adenocarcinoma with a decrease in the level of their differentiation. – (3+3), (3+4) i (4+4).

4. STATISTICAL ANALYSIS OF LAYER-BY-LAYER MAPS OF POLARIZATION ELLIPTICITY OF DIGITAL MICROSCOPIC IMAGES OF HISTOLOGICAL SECTIONS OF BIOPSY OF PROSTATE TUMORS WITH DIFFERENT DEGREES OF DIFFERENTIATION

The morphological scenarios of necrotic processes of oncological destruction are quantitatively illustrated by a set of mean intragroup values and standard deviations of the magnitude of statistical moments SM_i characterizing layer-by-layer distributions of the polarization ellipticity of digital microscopic images of representative samples of histological sections of adenoma biopsy (control group 1) and adenocarcinoma (experimental group 2 - group 4) different differentiation – (3+3), (3+4) and (4+4), - Table 1.

Table 1 Statistical parameters of layer-by-layer polarization ellipticity maps of microscopic images of histological sections of biopsy of benign and malignant prostate tumours

Type	Adenoma	Adenocarcinoma (3+3)	Adenocarcinoma (3+4)	Adenocarcinoma (4+4)
SM_1	0.21 ± 0.0095	0.17 ± 0.008	0.13 ± 0.006	0.099 ± 0.004
p	$p \le 0.001$			
		$p \le 0.05$		
			$p \le 0.05$	
SM_2	0.23 ± 0.0105	0.18 ± 0.008	0.15 ± 0.007	0.11 ± 0.005
p	$p \le 0.001$			
		$p \le 0.05$		
			$p \le 0.05$	
SM_3	0.46 ± 0.021	0.67 ± 0.029	0.89 ± 0.042	1.09 ± 0.049
p	$p \le 0.001$			
		$p \le 0.05$		
			$p \le 0.05$	
SM_4	0.55 ± 0.025	0.79 ± 0.037	1.08 ± 0.048	1.31 ± 0.063
p	$p \le 0.001$			
		$p \le 0.05$		
			$p \le 0.05$	

From the obtained data of the statistical analysis of the layer-by-layer distributions of the polarization ellipticity, which were determined by the method of polarization-interference mapping of a set of digital microscopic images, the statistical reliability of differentiation of all types of histological sections of biopsies of benign and malignant prostate tumours with varying degrees of differentiation according to the Gleason scale (3 + 3, 3 + 4 4 + 4) was established.

5. INFORMATIONAL ANALYSIS OF THE DIAGNOSTIC POWER OF THE METHOD OF 3D LAYER-BY-LAYER POLARIZATION-HOLOGRAPHIC MAPPING OF MICROSCOPIC IMAGES OF HISTOLOGICAL SECTIONS OF BIOPSY OF PROSTATE TUMOURS WITH DIFFERENT DEGREES OF DIFFERENTIATION

The following results were obtained:

- An excellent level of accuracy in the differential diagnosis “adenoma (control group 1) - adenocarcinoma (research group 2 – group 4)” – $Ac = 95\% \div 96\%$;
- Excellent level of accuracy of differential diagnosis "adenocarcinoma (3 + 3, - group 2) - adenocarcinoma (4 + 4, - group 4)” – $Ac = 93\% \div 91\%$;
- Excellent level of accuracy of differential diagnosis "adenocarcinoma (3 + 3, - group 2) - adenocarcinoma (3 + 4, - group 3)" – $Ac = 91\%$;
- Very good level of accuracy of differential diagnosis "adenocarcinoma (3 + 4, - group 3) - adenocarcinoma (4 + 4, - group 4)" – $Ac = 85\%$.

CONCLUSIONS

1. Possibilities of 3D Stokes-polarimetric mapping of microscopic images of protein fluorofores of the prostate with digital holographic reproduction of layer-by-layer polarization maps of ellipticity in the differential diagnosis of benign and malignant prostate tumours with different degrees of differentiation have been developed and investigated.
2. System 3D polarization-holographic measurements and statistical analysis of algorithmically reproducible layer-by-layer maps and histograms of the distribution of the polarization ellipticity of microscopic images of representative samples of prostate biological preparations were carried out.
3. A set of treatment-relevant relationships between the statistical moments of the 1st - 4th orders, which characterize the holographically reproduced layer-by-layer maps of distributions of the polarization ellipticity of digital microscopic images of a set of samples of representative samples of biological preparations, and pathological conditions of the prostate have been determined..
4. The operational characteristics (sensitivity, specificity, accuracy) of the diagnostic power of the method of 3D layer-by-layer Stokes-polarimetric mapping of the distributions of the polarization ellipticity of digital microscopic images of a protein fluorofores with pathological conditions of the prostate have been determined.

FUNDING

Current research supported by the National Research Foundation of Ukraine (Project 2020.02/0061)

REFERENCES

[1] V.V. Tuchin, Tissue Optics: Light Scattering Methods and Instruments for Medical Diagnosis, second edition, PM 166, SPIE Press, Bellingham, WA (2007).
[2] X. Wang, G. Yao, L. - H. Wang, “Monte Carlo model and single-scattering approximation of polarized light propagation in turbid media containing glucose,” Appl. Opt. 41, 792–801 (2002).
[3] X. Wang, L. - H. Wang, “Propagation of polarized light in birefringent turbid media: a Monte Carlo study,” J. Biomed. Opt. 7, 279-290 (2002).
[4] B N. Ghosh and I. A. Vitkin, “Tissue polarimetry: concepts, challenges, applications and outlook,” J. Biomed. Opt. 16, 110801 (2011).
[5] N. Ghosh, M. F. G. Wood, and I. A. Vitkin, “Polarized light assessment of complex turbid media such as biological tissues via Mueller matrix decomposition,” in Handbook of Photonics for Biomedical Science, V.V. Tuchin, Ed., pp. 253–282, CRC Press, Taylor & Francis Group, London (2010).
[6] H. H. Tynes et al., “Monte Carlo and multicomponent approximation methods for vector radiative transfer by use of effective Mueller matrix calculations,” Appl. Opt. 40(3), 400–412 (2001).
[7] N. G. Khlebtsov et al., “Introduction to light scattering by biological objects,” in Handbook of Optical Biomedical Diagnostics, 2nd ed., Vol. PM 262, pp. 1–155, V. V. Tuchin, Ed., SPIE Press, Bellingham, Washington (2016).
[8] Alexander G. Ushenko and Vasilii P. Pishak, “Laser Polarimetry of Biological Tissue: Principles and Applications”, in Handbook of Coherent-Domain Optical Methods: Biomedical Diagnostics, Environmental and Material Science, vol. I, Valery V. Tuchin, Ed. Boston: Kluwer Academic Publishers, 2004, pp. 93-138.
[9] O. V. Angelsky, A. G. Ushenko, Yu. A. Ushenko, V. P. Pishak, A. P. Peresunko, “Statistical, Correlation and Topological Approaches in Diagnostics of the Structure and Physiological State of Birefringent Biological Tissues” in Handbook of Photonics for Biomedical Science, pp. 283-322 ed. by Valery V. Tuchin, CRC PressTaylor&Francis group: Boca Raton, London, New York (2010).
[10] Angelsky, O.V., Zenkova, C.Y., Hanson, S.G., Zheng, J. Extraordinary Manifestation of Evanescent Wave in Biomedical Application (2020) Frontiers in Physics, 8, 159.
[11] Y. A. Ushenko, T. M. Boychuk, V. T. Bachynsky, O. P. Mincer, “Diagnostics of Structure and Physiological State of Birefringent Biological Tissues: Statistical, Correlation and Topological Approaches” in Handbook of Coherent-Domain Optical Methods, Springer Science+Business Media, p. 107, New York (2013).

[12] Ushenko, V.O., Trifonyuk, L., Ushenko, Y.A., Dubolazov, O.V., Gorsky, M.P., Ushenko, A.G. Polarization singularity analysis of Mueller-matrix invariants of optical anisotropy of biological tissues samples in cancer diagnostics (2021) Journal of Optics (United Kingdom), 23 (6), 064004.

[13] Meglinski, I., Trifonyuk, L., Bachinsky, V., Vanchulyak, O., Bodnar, B., Sidor, M., Dubolazov, O., Ushenko, A., Ushenko, Y., Soltys, I.V., Bykov, A., Hogan, B., Novikova, T. Polarization Correlometry of Microscopic Images of Polycrystalline Networks Biological Layer (2021) SpringerBriefs in Applied Sciences and Technology, pp. 61-73.

[14] Meglinski, I., Trifonyuk, L., Bachinsky, V., Vanchulyak, O., Bodnar, B., Sidor, M., Dubolazov, O., Ushenko, A., Ushenko, Y., Soltys, I.V., Bykov, A., Hogan, B., Novikova, T. Scale-Selective and Spatial-Frequency Correlometry of Polarization-Inhomogeneous Field (2021) SpringerBriefs in Applied Sciences and Technology, pp. 33-59.

[15] Meglinski, I., Trifonyuk, L., Bachinsky, V., Vanchulyak, O., Bodnar, B., Sidor, M., Dubolazov, O., Ushenko, A., Ushenko, Y., Soltys, I.V., Bykov, A., Hogan, B., Novikova, T. Multifunctional Stokes Correlometry of Biological Layers (2021) SpringerBriefs in Applied Sciences and Technology, pp. 75-96.

[16] Meglinski, I., Trifonyuk, L., Bachinsky, V., Vanchulyak, O., Bodnar, B., Sidor, M., Dubolazov, O., Ushenko, A., Ushenko, Y., Soltys, I.V., Bykov, A., Hogan, B., Novikova, T. Methods and Means of Polarization Correlation of Fields of Laser Radiation Scattered by Biological Tissues (2021) SpringerBriefs in Applied Sciences and Technology, pp. 1-15.

[17] Meglinski, I., Trifonyuk, L., Bachinsky, V., Vanchulyak, O., Bodnar, B., Sidor, M., Dubolazov, O., Ushenko, A., Ushenko, Y., Soltys, I.V., Bykov, A., Hogan, B., Novikova, T. Materials and Methods (2021) SpringerBriefs in Applied Sciences and Technology, pp. 17-31.

[18] Angelsky, O.V., Bekshaev, A.Y., Dragan, G.S., Maksimyak, P.P., Zenkova, C.Y., Zheng, J. Structured Light Control and Diagnostics Using Optical Crystals (2021) Frontiers in Physics, 9,715045.

[19] Angelsky, O.V., Maksimyak, P.P. Optical diagnostics of slightly rough surfaces (1992) Applied Optics, 31 (1), pp. 140-143

[20] Angelsky, O.V., Zenkova, C.Y., Hanson, S.G., Zheng, J. Extraordinary Manifestation of Evanescent Wave in Biomedical Application (2020) Frontiers in Physics, 8, 159.

[21] Trifonyuk, L., Sdobnov, A., Baranowski, W., Ushenko, V., Olar, O., Dubolazov, A., Pidkamin, L., Sidor, M., Vanchuliak, O., Motrich, A., Gorsky, M., Meglinski, I Differential Mueller matrix imaging of partially depolarizing optically anisotropic biological tissues (2020) Lasers in Medical Science, 35 (4), pp. 877-891.

[22] Angelsky, O.V., Bekshaev, A.Y., Hanson, S.G., Zenkova, C.Y., Mokhun, I.I., Jun, Z. Structured Light: Ideas and Concepts (2020) Frontiers in Physics, 8, 114.

[23] Angelsky, O.V., Ushenko, Y.A., Dubolazov, A.V., Telenha, O.Yu. The interconnection between the coordinate distribution of mueller-matrixes images characteristic values of biological liquid crystals net and the pathological changes of human tissues (2010) Advances in Optical Technologies, 130659

[24] Borovkova, M., Trifonyuk, L., Ushenko, V., Dubolazov, O., Vanchulyak, O., Bodnar, G., Ushenko, Y., Olar, O., Ushenko, O., Sakhnovskiy, M., Bykov, A., Meglinski, I. Mueller-matrix-based polarization imaging and quantitative assessment of optically anisotropic polycrystalline networks (2019) PLoS ONE, 14 (5), e0214494 .

[25] P. Wang, X. Zhang, Y. Xiang, F. Shi, M. Gavryliak, and J. Xu, "Random laser with superscatterers at designable wavelengths," Opt. Express 23, 24407-24415 (2015).